

Dalton Transactions

Accepted Manuscript



This is an *Accepted Manuscript*, which has been through the Royal Society of Chemistry peer review process and has been accepted for publication.

Accepted Manuscripts are published online shortly after acceptance, before technical editing, formatting and proof reading. Using this free service, authors can make their results available to the community, in citable form, before we publish the edited article. We will replace this *Accepted Manuscript* with the edited and formatted *Advance Article* as soon as it is available.

You can find more information about *Accepted Manuscripts* in the [Information for Authors](#).

Please note that technical editing may introduce minor changes to the text and/or graphics, which may alter content. The journal's standard [Terms & Conditions](#) and the [Ethical guidelines](#) still apply. In no event shall the Royal Society of Chemistry be held responsible for any errors or omissions in this *Accepted Manuscript* or any consequences arising from the use of any information it contains.

**Achieving near-infrared emission in platinum (II) complexes
by using an extended donor-acceptor-type ligand**

You-Ming Zhang,^a Fanyuan Meng,^{a,c} Jian-Hong Tang,^c Yafei Wang,^a Caifa You,^a Hua
Tan,^a Yu Liu,^a Yu-Wu Zhong,^{d,*} Shijian Su,^{c*} and Weiguo Zhu^{a,b*}

^a *College of Chemistry, Xiangtan University, Key Lab of Environment-Friendly
Chemistry and Application in Ministry of Education,*

Xiangtan 411105, China.

^b *School of Materials Science and Engineering, Changzhou University, Changzhou
213164, China*

^c *Institute of Polymer Optoelectronic Materials and Devices, State Key Laboratory of
Luminescent Materials and Devices, South China University of Technology,
Guangzhou 510640, China.*

^d *Beijing National Laboratory for Molecular Sciences, CAS Key Laboratory of
Photochemistry, Institute of Chemistry, Chinese Academy of Sciences,
Beijing 100190, China.*

Email addresses:

(W. Z) zhuwg18@126.com,

(S. S) mssjsu@scut.edu.cn,

(Y.-W.Z.) zhongyuwu@iccas.ac.cn

Abstract: A series of the C^N ligand with donor-acceptor (D-A) frameworks, i.e. TPA-BTPy, TPA-BTPy-Fl and Fl(TPA-BTPy)₂, as well as their mono- and di-nuclear platinum (II) complexes of (TPA-BTPy)Pt(pic), (TPA-BTPy-Fl)Pt(pic) and [Fl(TPA-BTPy)₂]Pt₂(pic)₂, are respectively designed and synthesized, in which triphenylamine (TPA) and fluorene (Fl) are used as the D units, 4-(pyrid-2-yl)benzothiadiazole (BTPy) as the A unit, and picolate anion (pic) as the auxiliary ligand. Their thermal, photophysical and electrochemical characteristics were investigated. Compared to mono-nuclear platinum complexes and their free ligands, this di-nuclear one of [Fl(TPA-BTPy)₂]Pt₂(pic)₂ shows an obvious interaction from platinum atom to ligand and dual emission peaks at 828 and 601 nm in thin films. Upon oxidation with antimony pentachloride in dichloromethane, charge transfer transitions between platinum and ligand are observed for the three complexes. The single-emissive-layer polymer light-emitting devices doped with [Fl(TPA-BTPy)₂]Pt₂(pic)₂ display a strong electroluminescence with dual emission peaks at 780 and 600 nm at a dopant concentration over 4 wt%. The maximum external quantum efficiency of 0.02% with a radiance of 59 μW/cm⁻² is obtained in the device at 30 wt% dopant concentration. This work indicates that the use of an extended D-A-type ligand is an effective strategy to achieve NIR emission for platinum complexes in PLEDs.

Keywords: Near-infrared emission, donor-accepter, platinum (II) complexes, electroluminescence.

1. Introduction

Near-infrared (NIR) luminescent organic compounds are an emerging class of materials with potential applications in night-vision displays, sensors, optical communication, and medical treatments [1-5]. To date, much efforts have been made to develop NIR-emitting materials with emission wavelength longer than 700 nm, such as boron dipyrromethene dyes [6], fluorescent compounds with a donor-acceptor (D-A) structure [7], lanthanide complexes [8] and transition metal complexes [9]. Among these materials, transition metal complexes have the potential to exhibit higher emission efficiency due to the strong spin-orbit coupling of heavy metals [10-15]. Metalloporphyrin, one of the representative examples, has recorded an external quantum efficiency (*EQE*) maximum of 3.0% for polymer light-emitting devices (PLEDs) and 9.2% for organic light-emitting devices (OLEDs) with NIR emission at 760-780 nm [16]. However, few platinum (II) complexes besides Pt-porphyrin compounds have displayed efficient NIR emission although highly efficient red, green, blue and even white emissions in OLEDs have been realized by tuning the molecular structures of square planar platinum (II) complexes [17-19]. In order to study the structure-property relationship, Gao *et al.* reported a mononuclear platinum complex of (phpy)Pt(q) (phpy=2-phenylpyridine; q=8-hydroxyquinoline), which displayed an electroluminescence (EL) peak at 675 nm and three shoulders at 690, 780 and 820 nm [20]. Che *et al.* reported a series of neutral mononuclear platinum complexes containing substituted 8-hydroxyquinoline, which gave a deep-red emission band from 650 to 695 nm with another weak NIR emission band from 705 to 755 nm in the device with an *EQE* of 1.7% [21].

In contrast to platinum complexes, most NIR-emitting organic and polymeric fluorescent dyes are built with electron-donating (D) units and electron-accepting (A)

units. Their band gap levels and photoelectronic properties can be readily tuned through a systematic variation between the D and A units [22-26]. Furthermore, hybridizations of the energy levels between the D and A units can modulate the highest occupied molecular orbit (HOMO) and the lowest unoccupied molecular orbit (LUMO) energy levels, which lead to a narrow HOMO-LUMO energy separation and shift of the emission energy to the NIR region [1]. For example, Wang *et al.* reported a class of D- π -A- π -D-type fluorescent dyes, which displayed emission at 1080 nm with an EQE of 0.28% in the OLEDs [7]. Cacialli *et al.* reported a kind of low-gap conjugated polymer with D-A structure, which displayed an emission peak at 956 nm with quantum efficiency of 0.04% [27].

In consideration of the merits of platinum complexes and D-A-type fluorescent dyes, we previously synthesized a mononuclear platinum complex of (Piq-G)Pt(acac) (Piq-G = 1-phenylisoquinoline derivative; acac = acetyl acetonate) with D-A chromophores, which exhibited a main emission band at 640 nm with a shoulder peak at 700 nm. Compared to the parent platinum (II) complex of (Piq)Pt(acac) (Piq = 1-phenylisoquinoline), (Piq-G)Pt(acac) presented a distinct red-shifted emission (40-60 nm) [28]. In order to develop new NIR-emitting materials and further study the effect of molecular structures of platinum complexes on their photophysical and electrochemical properties, three platinum complexes with D-A, D-A-D or D-A-D-A-D-type C^N ligand have been synthesized in this work. The made C^N ligand with donor-acceptor (D-A) frameworks are abbreviated as TPA-BTPy, TPA-BTPy-Fl and Fl(TPA-BTPy)₂, in which TPA, BTPy, Fl and pic represent triphenylamine, 4-(pyrid-2-yl) benzothiazole, pyridine, fluorine and picolate anion, respectively. Their corresponding mono- and di-nuclear platinum complexes are abbreviated as (TPA-BTPy)Pt(pic), (TPA-BTPy-Fl)Pt(pic) and [Fl(TPA-BTPy)₂]Pt₂(pic)₂, respectively in Figure 1. Their

synthetic routes are shown in Scheme 1. As the non-planar TPA donor unit is available to improve carrier-transporting property and suppress molecular aggregation, as well as the BT unit is a common class of luminescence units in OLEDs and acceptor units in organic solar cells reported in recent years ^[29-31], this class of platinum complexes is possible to give NIR emission by the intramolecular D-A interaction. Interestingly, two mono-nuclear platinum complexes of (TPA-BTPy)Pt(pic) and (TPA-BTPy-FI)Pt(pic) only gave red emission under photoexcitation in dichloromethane (DCM) solution and thin films. The dinuclear platinum complex of [FI(TPA-BTPy)₂]Pt₂(pic)₂ displayed red emission in its DCM solution, but NIR emission was observed at 828 nm in its thin film at room temperature. To further understand these unusual phenomena, three platinum complexes were oxidized and corresponding NIR absorption spectral changes were analyzed ^[32-36]. Our work indicates that changing the D-A framework of the C^N ligands can tune the optoelectronic properties and emission wavelength of platinum complexes, thus provide a potential to realize NIR emissions.

2. Results and discussions

2.1 Synthesis

All solvents were carefully dried and distilled prior to use. Commercially available reagents were used without further purification unless otherwise stated. All reactions were performed under nitrogen atmosphere and monitored by thin-layer chromatography. As shown in Scheme 1, *N,N*-diphenyl-4-(4,4,5,5-tetramethyl-1,3,2-dioxaborolan-2-yl)benzenamine (TPA-BPin) was synthesized by referring to the reported procedure ^[29]. TPA-BT-Br, TPA-BT-BPin, TPA-BTPy, TPA-BTPy-Br, and TPA-BTPy-FI were synthesized by a similar Suzuki coupling reaction using PdCl₂(dppf) or

$\text{Pd}(\text{PPh}_3)_4$ as a catalyst with a high yield. $(\text{TPA-BTPy-Br})\text{Pt}(\text{pic})$, $(\text{TPA-BTPy})\text{Pt}(\text{pic})$ and $(\text{TPA-BTPy-Fl})\text{Pt}(\text{pic})$ were synthesized using the previous method with two-step procedures, including a cyclometalation of TPA-BTPy-Br, TPA-BTPy and TPA-BTPy-Fl and a chloride cleavage of their corresponding dimers with picolinic acid [28]. $[\text{Fl}(\text{TPA-BTPy})_2]\text{Pt}_2(\text{pic})_2$ was synthesized by the Suzuki coupling reaction using $\text{Pd}(\text{PPh}_3)_4$ as a catalyst and cesium carbonate as a base with a yield of 31%. The detailed synthesis and characterization of the three platinum complexes are given in the experimental section. All new compounds in this contribution were fully characterized with ^1H NMR, ^{13}C NMR, MALDI-TOF mass spectra and elemental analysis.

2.2 Thermal property

The thermo-gravimetric analyses (TGA) curves of three platinum complexes under N_2 atmosphere are depicted in Figure. 2 and the corresponding data are summarized in Table 1. The decomposition temperature (T_d) of 315 °C for $(\text{TPA-BTPy})\text{Pt}(\text{pic})$, 317 °C for $(\text{TPA-BTPy-Fl})\text{Pt}(\text{pic})$ and 296 °C for $[\text{Fl}(\text{TPA-BTPy})_2]\text{Pt}_2(\text{pic})_2$ were observed at a 5% weight loss under N_2 protection, respectively. It indicates that $[\text{Fl}(\text{TPA-BTPy})_2]\text{Pt}_2(\text{pic})_2$ with D(A-D)₂ framework displays a slightly decreased thermal stability than two mono-nuclear platinum complexes with D-A and D-A-D frameworks..

2.3 Electrochemical properties

The cyclic voltammetry (CV) curves of three platinum complexes and their free C^N ligands in films coated on a platinum electrode are shown in Figure 3 and Figure S2 (see ESI). The resulting electrochemical data are summarized in Table 1. The onset of oxidation/reduction potentials ($E_{\text{ox}}/E_{\text{red}}$) of 0.98 /-1.22 , 0.93 /-1.17 , 0.77 /-1.02 , 1.07 /-0.85, 1.06 /-0.93 and 0.88 /-0.95 (V/V) are respectively observed for the C^N ligands of TPA-BTPy, TPA-BTPy-Fl, $[\text{Fl}(\text{TPA-BTPy})_2]$ and their platinum complexes

of (TPA-BTPy)Pt(pic), (TPA-BTPy-FI)Pt(pic), [FI(TPA-BTPy)₂]Pt₂(pic)₂. It shows that platinum complexes exhibit an increased oxidation/reduction potentials compared to their corresponding C^N ligands. Furthermore, this dinuclear platinum complex presents a lower oxidation/reduction potentials than the mono-nuclear platinum complexes. As the HOMO and LUMO energy levels (E_{HOMO} and E_{LUMO}) can be estimated by the $E_{\text{ox}}/E_{\text{red}}$ values based on the empirical equations of $E_{\text{HOMO}} = [- (E_{\text{ox}} - 0.45) - 5.1]$ and $E_{\text{LUMO}} = [- (E_{\text{red}} - 0.45) - 5.1]$ eV, in which 0.45 V is a potential of ferrocene vs. Ag/AgCl and 5.1 eV is the energy level of ferrocene versus the vacuum energy level, thus, the $E_{\text{HOMO}}/E_{\text{LUMO}}$ values of -5.63/-3.43 eV for TPA-BTPy, -5.58/-3.48 eV for TPA-BTPy-FI, -5.42/-3.67 eV for FI(TPA-BTPy)₂, -5.72/-3.80 eV for (TPA-BTPy)Pt(pic), -5.71/-3.75 eV for (TPA-BTPy-FI)Pt(pic) and -5.53/-3.72 eV for [FI(TPA-BTPy)₂]Pt₂(pic)₂ are obtained. It is found that [FI(TPA-BTPy)₂]Pt₂(pic)₂ exhibits a decreased electrochemical band gap of 1.81 eV and a decreasing HOMO energy level. Therefore, introducing D(A-D)₂ framework in [FI(TPA-BTPy)₂]Pt₂(pic)₂ is in favour of lowering band gap and can make red-shifted emission.

2.4 Photophysical properties and time-dependent DFT (TDDFT) calculations.

The UV-Vis absorption spectra of three platinum complexes in DCM solution and in neat films are presented in Figure. 4, as well as the time-dependent density functional theory (TDDFT) calculations for [FI(TPA-BTPy)₂]Pt₂(pic)₂, together with orbitals and data are given in Figure S1 and Table S1 in Supporting Information (SI). The corresponding absorption data are listed in Table 2. In solution state, three platinum complexes exhibit similar UV spectra with three absorption bands. According to the TDDFT calculated results, the high-lying band from 300 nm to 400 nm are assigned to the π - π^* transitions of their conjugated backbones, mainly associated with S_{21} , S_{23} , S_{26} , S_{29} , S_{31} , S_{37} and S_{40} excitations. The moderate-lying band at about 430 nm

is mainly attributed to the mixed spin-allowed and spin-forbidden singlet $^1\text{MLCT}$ and $^3\text{MLCT}$ transitions, mainly associate with S_6 , S_7 , S_{10} , S_{12} , S_{15} and S_{16} . The low-lying band at about 500 nm originates from the intramolecular charge transfer (ICT) transitions from the TPA to the BTPy unit, which is dominated by the HOMO-1 \rightarrow LUMO+1. Furthermore, the ICT transitions with the maximum molar absorption coefficient (ϵ) value of $4.57 \times 10^4 \text{ M}^{-1} \text{ cm}^{-1}$ for $[\text{Fl}(\text{TPA-BTPy})_2]\text{Pt}_2(\text{pic})_2$, which is 2.0 and 3.1 times higher than those values of $(\text{TPA-BTPy})\text{Pt}(\text{pic})$ and $(\text{TPA-BTPy-Fl})\text{Pt}(\text{pic})$, respectively. The increased absorption intensity of $[\text{Fl}(\text{TPA-BTPy})_2]\text{Pt}_2(\text{pic})_2$ is due to its enlarged D-A system. In solid state, three platinum complexes shows about 20 nm red-shifted absorption profiles in comparison to those in solution due to the enhanced intermolecular π - π stacking effect. Based on the onset of film absorption profiles, the optical band gaps (E_{opt}^g) of $(\text{TPA-BTPy})\text{Pt}(\text{pic})$, $(\text{TPA-BTPy-Fl})\text{Pt}(\text{pic})$ and $[\text{Fl}(\text{TPA-BTPy})_2]\text{Pt}_2(\text{pic})_2$ are calculated to be 2.13 eV, 2.06 eV and 2.05 eV, respectively.

The photoluminescence spectra of three platinum complexes in DCM solution and neat films are presented in Figure 5. The corresponding absorption data are listed in Table 2. In solution state, under photo-excitation at 500 nm, three platinum complexes displayed a similar PL spectrum with an emission peak at about 640 nm. Compared to PL spectra of the TPA-BTPy, TPA-BTPy-Fl, and $\text{Fl}(\text{TPA-BTPy})_2$ ligand (Figure S3), we speculate that the emission of these platinum complexes originates from the intrinsic emission of their intra-ligands. In the solid state, two mono-nuclear platinum complexes of $(\text{TPA-BTPy})\text{Pt}(\text{pic})$ and $(\text{TPA-BTPy-Fl})\text{Pt}(\text{pic})$ only gave red emission. However, the dinuclear complex of $[\text{Fl}(\text{TPA-BTPy})_2]\text{Pt}_2(\text{pic})_2$ exhibited a remarkable NIR emission peak at 828 nm besides red emission at 601 nm at room temperature. It indicates that the dinuclear platinum complex constructed with dual D-A system is

able to exhibit NIR emission in the solid film. The NIR emission phenomenon of $[\text{Fl}(\text{TPA-BTPy})_2]\text{Pt}_2(\text{pic})_2$ prompted us to further explore its electroluminescent characteristics.

2.5 NIR absorption analysis upon one-electron oxidation

To further probe the electronic delocalization of $(\text{TPA-BTPy})\text{Pt}(\text{pic})$, $(\text{TPA-BTPy-Fl})\text{Pt}(\text{pic})$ and $[\text{Fl}(\text{TPA-BTPy})_2]\text{Pt}_2(\text{pic})_2$, the UV-vis and NIR absorption spectral changes of three free C^N ligands and their platinum complexes were monitored upon stepwise oxidation with SbCl_5 in DCM (Figures S4 – S9). For the three C^N ligands, upon the gradual addition of SbCl_5 , the TPA units in TPA-BTPy, TPA-BTPy-Fl and $[\text{Fl}(\text{TPA-BTPy})_2]$ are stepwise oxidized to N^+ . Meanwhile, a new absorption band at 550 ~ 590 nm is appeared and increased caused by a new intramolecular charge transfer (ICT) transitions from the TPA radical cation to the BTPy unit. With further addition of SbCl_5 , a new absorption band at about 800 nm is appeared, which results from a typical triarylamine radical cation^[33]. When an excess of the oxidant is added, no more changes are evident.

For platinum (II) complexes, upon the gradual addition of SbCl_5 , the TPA units in $(\text{TPA-BTPy})\text{Pt}(\text{pic})$ and $(\text{TPA-BTPy-Fl})\text{Pt}(\text{pic})$ are stepwise oxidized to N^+ , as evidenced by the emergence of a new absorption band about 800 nm arising from a typical triarylamine radical cation specie. At the same time, a weak absorption band at 1600 nm appears, which is assigned to charge transfer transition from the metal component to the triarylamine center ($\text{Pt} \rightarrow \text{N}^+$). With further addition of SbCl_5 , the absorption at 1600 nm decrease, but the N^+ -associated absorption is continued to increase. When an excess of the oxidant is added, no more changes are evident.

It is noted that $[\text{Fl}(\text{TPA-BTPy})_2]\text{Pt}_2(\text{pic})_2$ with two redox-active amine sites and two platinum units exhibits somewhat different absorption spectral changes upon oxida-

tion. Upon the gradual addition of SbCl_5 , $[\text{Fl}(\text{TPA-BTPy})_2]\text{Pt}_2(\text{pic})_2$ displays a much stronger absorption peak at 1600 nm without the N^+ -associated absorption band. With a further increase in the amount of SbCl_5 , the peak at 1600 nm decreases. At the same time, the N^+ -associated absorption appears and continuously increases. Figure 6 shows the UV-vis and NIR electronic absorption spectra of three platinum complexes after one oxidation by SbCl_5 . Taking into account the above oxidative titration measurements, we believe that the interaction between metal and ligand for the dinuclear platinum complex of $[\text{Fl}(\text{TPA-BTPy})_2]\text{Pt}_2(\text{pic})_2$ is stronger than that for the mononuclear platinum complexes of $(\text{TPA-BTPy})\text{Pt}(\text{pic})$ and $(\text{TPA-BTPy-Fl})\text{Pt}(\text{pic})$.

In many studies on mixed-valence systems, DFT and TDDFT calculations were performed on the open-shell substances to provide insight into the spin-density distribution and the nature of intervalence-charge-transfer (IVCT) bands^[37,38]. Using the same method (B3LYP/Lanl2DZ/6-31G*/CPCM), we have carried out similar calculations on the basis of the previously DFT optimized structure of complexes after changing the charge to +1 and the spin multiplicity to +2. The isodensity plots of the highest occupied spin orbitals (HOSO) of three platinum complexes are shown in Figure 7, which are involved in the above transitions. The spin density is mainly dominated by triphenylamine and platinum ions in these platinum complexes. The NIR excitations at 1425 nm for $(\text{TPA-BTPy})\text{Pt}(\text{pic})$, 1890 nm for $(\text{TPA-BTPy-Fl})\text{Pt}(\text{pic})$, and 1913 nm for $[\text{Fl}(\text{TPA-BTPy})_2]\text{Pt}_2(\text{pic})_2$ are mainly associated with the S_1 , S_2 , and S_2 transitions, respectively. Based on these results, we believe that amine is oxidized first and behave as the acceptor for the $\text{Pt} \rightarrow \text{N}^+$ MLCT transitions, which lead to an NIR absorption at ~ 1600 nm. Furthermore, the oxidized ligand behaves as a stronger acceptor in $[\text{Fl}(\text{TPA-BTPy})_2]\text{Pt}_2(\text{pic})_2$ for the $\text{Pt} \rightarrow \text{N}^+$ MLCT transitions after the two triphenylamine units were simultaneously oxidized. When platinum is oxidized

gradually, the N^+ -associated absorption is released and increases, which result in decrease of the peak at 1600 nm.

2.6 Electroluminescence Properties

Taking into account above analysis, we only used $[Fl(TPA-BTPy)_2]Pt_2(pic)_2$ as dopant to make PLEDs and further study its EL properties. Figure 8 shows the EL spectra of the $[Fl(TPA-BTPy)_2]Pt_2(pic)_2$ -doped devices at different dopant concentrations from 20 wt% to 30 wt%. The EL spectra at low dopant concentrations from 1 wt% to 16 wt% are shown in Figure S10. Three distinct EL peaks at about 460 nm, 600 nm and 780 nm are observed, which are assigned to the PVK-OXD-7, the $Fl(TPA-BTPy)_2$ ligand center (LC) and $[Fl(TPA-BTPy)_2]Pt_2(pic)_2$ emissions compared to the EL spectra of the $Fl(TPA-BTPy)_2$ -doped devices in Figure S11. At low doping concentrations from 1 wt% to 2 wt%, the EL is simultaneously dominated by PVK-OXD-7 and $Fl(TPA-BTPy)_2$ emissions. With further increasing dopant concentrations, the PVK-OXD-7 emission is quickly decreased, and the $[Fl(TPA-BTPy)_2]Pt_2(pic)_2$ emission is gradually enhanced. The gradually enhanced emission at dopant concentrations from 1 wt% to 30 wt% at 780 nm might come from excimers and/or exciplexes except the intrinsic emission of $[Fl(TPA-BTPy)_2]Pt_2(pic)_2$ [39]. When the dopant concentration is 4.0 wt%, the PVK-OXD-7 emission is almost quenched and strong NIR emission from $[Fl(TPA-BTPy)_2]Pt_2(pic)_2$ appears.

Figure 9 shows the current densities-voltage ($J-V$) and radiant emittance curves of the devices from 20 wt% to 30 wt% dopant concentrations. The corresponding device performance data are summarized in Table 3. The turn-on voltage of the devices is under around 8 V without drastic change. It indicates that the devices are not operated by the carrier-trapping mechanism based on the identical phenomenon observed previously by Chang *et al* [40]. The highest radiant intensity of 41, 49 and $59\mu W cm^{-2}$ are

obtained in the devices at the doping concentrations 20 wt%, 24 wt% and 30 wt%, respectively. Figure 10 shows the EQE - J characteristic of the $[Fl(TPA-BTPy)_2]Pt_2-(pic)_2$ -doped devices at different dopant concentrations from 20 wt% to 30 wt%. The corresponding device performance data are summarized in Table 3. The maximum EQE of 0.02% at current density of 5.46 mA cm^{-2} is observed in the devices at the dopant concentration of 30 wt%. It is worth to note that the devices exhibit an increasing EQE with increasing dopant concentrations, indicates introducing bulky nonplanar TPA unit into D-A structure can suppress dopant concentration quenching. Furthermore, the EQE level displays small roll-off at high current densities. This sluggish roll-off is favorable for practical applications of OLEDs^[41]. We note that many cyclometalated platinum complexes usually gave the same phenomenon in the devices because this class of planar platinum complexes has relatively long lifetimes, which easily result in the dominant exciton decay channel by triplet-triplet annihilation (TTA).

3. Conclusions

In summary, a class of new D-A-type mono- and di-nuclear platinum (II) complexes of $(TPA-BTPy)Pt(pic)$, $(TPA-BTPy-Fl)Pt(pic)$ and $[Fl(TPA-BTPy)_2]Pt_2-(pic)_2$ were synthesized and characterized. Different coupling intensity between ligand and platinum were observed by one-electron oxidation of these platinum complexes with antimony pentachloride. The interaction between metal and ligand for $[Fl(TPA-BTPy)_2]Pt_2(pic)_2$ is stronger with respect to that of $(TPA-BTPy)Pt(pic)$ and $(TPA-BTPy-Fl)Pt(pic)$. The NIR emission peaks at 826 nm and 780 nm were only observed for the $[Fl(TPA-BTPy)_2]Pt_2(pic)_2$ film under photo-excitation and for the $[Fl(TPA-BTPy)_2]Pt_2-(pic)_2$ -doped PLEDs under electric field, respectively. The maximum EQE of 0.02% with an irradiance intensity of $59 \mu\text{W cm}^{-2}$ was obtained in the $[Fl(TPA-BTPy)_2]Pt_2-$

(pic)₂-doped PLEDs at 30 wt% dopant concentration.

4. Experiment section

Synthesis

1. 4-(7-bromobenzo[c][1,2,5]thiadiazol-4-yl)-*N,N*-diphenylbenzenamine (**TPA-BT-Br**)

To a mixture of *N,N*-diphenyl-4-(4,4,5,5-tetramethyl-1,3,2-dioxaborolan-2-yl) benzenamine (TPA-Bpin, 1326 mg, 3.86 mmol), 4,7-dibromobenzo[c][1,2,5] thiadiazole (1350 mg, 4.64 mmol) and tetrakis(triphenylphosphine) palladium (Pd(PPh₃)₄, 224 mg) was added a degassed mixture of toluene (30 mL), anhydrous ethanol (5 mL) and 2 M potassium carbonate aqueous solution (6 mL). The mixture was refluxed for 23 h under the protection of nitrogen. After cooled to room temperature, the mixture was poured into water (100 mL). It was extracted with DCM (3 × 50 mL) and the combined organic layer was dried over anhydrous magnesium sulfate. The solvent was removed off by rotary evaporation and the residue was passed through a flash silica gel column with petroleum ether / dichloromethane (PE-DCM, *V/V*, 3:1) as the eluent to give a orange red solid (2.01 g, yield 82%). ¹H NMR (400 MHz, CDCl₃), δ (ppm): 7.90 (d, *J* = 7.6 Hz, 1H), 7.81 (d, *J* = 8.5 Hz, 2H), 7.55 (d, *J* = 7.6 Hz, 1H), 7.31-7.25 (m, 5H), 7.17 - 7.19 (d, *J* = 6.5 Hz, 5H), 7.08 (t, *J* = 7.2 Hz, 2H). MALDI-MS (*m/z*): 459.067 for [M⁺]. ¹³C NMR (100 MHz, CDCl₃), δ (ppm): 112.2, 122.7, 123.6, 125.1, 127.3, 129.4, 130.0, 132.4, 133.6, 147.4, 148.5, 153.2, 154.0.

2. *N,N*-diphenyl-4-(7-(4,4,5,5-tetramethyl-1,3,2-dioxaborolan-2-yl)benzo[c][1,2,5]thiadiazol-4-yl)benzenamine (**TPA-BT-BPin**)

To 40 mL dry tetrahydrofuran were added TPA-BT-Br (813 mg, 1.78 mmol), bis(pinacolato) diboron (1807 mg, 7.12 mmol), potassium acetate (872 mg, 8.90 mmol) and [1,10-bis(diphenylphosphino)-ferrocene] dichloropalladium (390 mg, 0.53

mmol). The mixture was reflux for 20 h under the protection of nitrogen. After cooled to room temperature, the mixture was extracted with DCM (3×50 mL) and the combined organic layer was dried over anhydrous magnesium sulfate. The solvent was removed off by rotary evaporation and the residue was passed through a flash silica gel column with PE-DCM (V/V , 1:1) as the eluent to give a orange red solid (674 mg, yield 75%). ^1H NMR (400 MHz, CDCl_3), δ (ppm): 8.23 (d, $J = 6.9$ Hz, 1H), 7.88 (d, $J = 8.4$ Hz, 2H), 7.68 (d, $J = 7.0$ Hz, 1H), 7.29 (t, $J = 7.7$ Hz, 4H), 7.19 (dd, $J = 7.5, 4.4$ Hz, 6H), 7.07 (t, $J = 7.2$ Hz, 2H), 1.46 (s, 12H). MALDI-MS (m/z): 505.290 for $[\text{M}^+]$. ^{13}C NMR (100 MHz, CDCl_3), δ (ppm): 24.6, 24.9, 25.0, 29.7, 83.5, 84.3, 122.7, 123.4, 125.0, 126.2, 129.4, 130.2, 130.8, 136.8, 139.2, 147.5, 148.5, 153.3, 158.4.

3. *N, N*-diphenyl-4-(7-(pyridin-2-yl)benzo[*c*][1,2,5]thiadiazol-4-yl)benzenamine (*TPA-BTPy*)

To a mixture of TPA-BT-Bpin (505 mg, 1.00 mmol), 2-bromopyridine (188 mg, 1.2 mmol) and $\text{Pd}(\text{PPh}_3)_4$ (60 mg) was added a degassed mixture of toluene (30 mL), anhydrous ethanol (6 mL) and 2 M potassium carbonate aqueous solution (5 mL). The mixture was refluxed for 12 h under the protection of nitrogen. After cooled to room temperature, the mixture was poured into water (50 mL). The purified procedure was similar to that of TPA-BT-Br using PE-DCM (V/V , 4:1) as the eluent to give a red solid (328 mg, yield 72%). ^1H NMR (400 MHz, CDCl_3) δ 8.79 (s, 1H), 8.68 (d, $J = 7.7$ Hz, 1H), 8.51 (d, $J = 6.9$ Hz, 1H), 7.90 (d, $J = 7.4$ Hz, 4H), 7.84 (d, $J = 7.0$ Hz, 1H), 7.31 (d, $J = 7.5$ Hz, 4H), 7.24 (d, $J = 12.4$ Hz, 4H), 7.19 (s, 2H), 7.08 (d, $J = 6.3$ Hz, 2H). MALDI-MS (m/z): 457.247 for $[\text{M}^+]$. ^{13}C NMR (100 MHz, CDCl_3), δ (ppm): 122.8, 122.9, 123.4, 124.9, 125.0, 127.3, 129.4, 129.8, 130.2, 130.7, 134.4, 136.6, 147.4, 148.3, 149.8, 153.7, 154.2.

4. 4-(7-(5-bromopyridin-2-yl)benzo[c][1,2,5]thiadiazol-4-yl)-*N,N*-diphenylbenzenamine (**TPA-BTPy-Br**)

To a mixture of TPA-BT-Bpin (820 mg, 1.72 mmol), 2,5-dibromopyridine (608 mg, 2.58 mmol) and Pd(PPh₃)₄ (100 mg) was added a degassed mixture of toluene (30 mL), anhydrous ethanol (6 mL) and 2 M potassium carbonate aqueous solution (5 mL). The mixture was refluxed for 20 h under the protection of nitrogen. The purified procedure was similar to that of TPA-BT-Br using PE-DCM (*V/V*, 2:1) as the eluent to give a red solid (569 mg, yield 62%). ¹H NMR (400 MHz, CDCl₃) δ (ppm): 8.82 (s, 1H), 8.73 (d, *J* = 8.4 Hz, 1H), 8.57 (d, *J* = 7.3 Hz, 1H), 8.00 (d, *J* = 8.4 Hz, 1H), 7.90 (d, *J* = 8.0 Hz, 3H), 7.83 (d, *J* = 7.4 Hz, 1H), 7.29 (d, *J* = 6.9 Hz, 4H), 7.20 (d, *J* = 5.4 Hz, 6H), 7.08 (t, *J* = 7.1 Hz, 2H). MALDI-MS (*m/z*): 534.113 for [M⁺]. ¹³C NMR (100 MHz, CDCl₃) δ (ppm): 119.9, 122.7, 123.5, 125.1, 125.8, 127.2, 128.8, 129.4, 129.8, 130.1, 130.5, 134.9, 147.5, 148.5, 150.7, 152.5, 153.5, 154.3.

5. 4-(7-(5-(9,9-dimethyl-9H-fluoren-2-yl)pyridin-2-yl)benzo[c][1,2,5]thiadiazol-4-yl)-*N,N*-diphenylbenzenamine (**TPA-BTPy-Fl**)

To a mixture of TPA-BTPy-Br (244 mg, 0.46 mmol), 2-(9,9-dimethyl-9H-fluoren-2-yl)-4,4,5,5-tetramethyl-1,3,2-dioxaborolane (175 mg, 0.55 mmol) and Pd(PPh₃)₄ (21 mg) was added a degassed mixture of toluene (25 mL), anhydrous ethanol (4 mL) and 2 M potassium carbonate aqueous solution (1 mL). The mixture was refluxed for 5 h under the protection of nitrogen. The purified procedure was similar to that of TPA-BT-Br using PE-DCM (*V/V*, 3:1) as the eluent to give a red solid (225 mg, yield 76%). ¹H NMR (400 MHz, CDCl₃) δ 9.17 (s, 1H), 8.90 (d, *J* = 8.0 Hz, 1H), 8.67 (d, *J* = 7.2 Hz, 1H), 8.23 (d, *J* = 8.1 Hz, 1H), 8.00 (d, *J* = 7.7 Hz, 2H), 7.94 (d, *J* = 7.4 Hz, 2H), 7.86 (d, *J* = 6.1 Hz, 1H), 7.81 (s, 1H), 7.75 (d, *J* = 7.5 Hz, 1H), 7.56 (d, *J* = 5.7

Hz, 1H), 7.45 (s, 2H), 7.38 (t, $J = 7.2$ Hz, 4H), 7.31 (d, $J = 7.5$ Hz, 2H), 7.28 (d, $J = 8.1$ Hz, 4H), 7.15 (t, $J = 6.8$ Hz, 2H), 1.64 (s, 6H). MALDI-MS (m/z): 649.269 for $[M^+]$. ^{13}C NMR (100 MHz, CDCl_3), 27.3, 47.1, 120.3, 120.7, 121.3, 122.7, 122.8, 123.5, 124.7, 125.0, 126.2, 127.2, 127.4, 127.7, 129.4, 129.6, 130.1, 134.4, 134.8, 136.0, 139.5, 147.5, 148.2, 148.3, 152.7.

6. *Fl(TPA-BTPy)₂*

To a mixture of TPA-BTPy-Br (241 mg, 0.45 mmol), 2-(9,9-dioctyl-7-(4,4,5,5-tetramethyl-1,3,2-dioxaborolan-2-yl)-9H-fluoren-2-yl)-4,4,5,5-tetramethyl-1,3,2-dioxaborolane (116 mg, 0.18 mmol) and $\text{Pd}(\text{PPh}_3)_4$ (20 mg) was added a degassed mixture of toluene (10 mL), anhydrous ethanol (3 mL) and 2 M potassium carbonate aqueous solution (1 mL). The mixture was refluxed for 23 h under the protection of nitrogen. The purified procedure was similar to that of TPA-BT-Br using DCM-EA (V/V , 20:1) as the eluent to give a red solid (160 mg, yield 69%). ^1H NMR (500 MHz, CDCl_3), δ (ppm): 9.13 (d, $J = 2.3$ Hz, 2H), 8.85 (d, $J = 8.2$ Hz, 2H), 8.61 (d, $J = 7.5$ Hz, 2H), 8.18 (dd, $J = 8.3, 2.4$ Hz, 2H), 7.94 (s, 2H), 7.92 (d, $J = 2.5$ Hz, 2H), 7.91 – 7.86 (m, 4H), 7.72 (d, $J = 9.3$ Hz, 2H), 7.69 (s, 2H), 7.31 (d, $J = 15.8$ Hz, 8H), 7.22 (dd, $J = 12.6, 8.1$ Hz, 12H), 7.08 (t, $J = 7.3$ Hz, 4H), 2.10 (dd, $J = 11.6, 4.7$ Hz, 4H), 1.28 – 1.06 (m, 24H), 0.80 (d, $J = 7.0$ Hz, 6H). MALDI-MS (m/z): 1299.933 for $[M^+]$. ^{13}C NMR (100 MHz, CDCl_3), δ (ppm): 14.1, 22.6, 24.0, 29.3, 30.1, 31.9, 40.4, 55.5, 120.7, 122.8, 123.5, 124.7, 125.0, 127.4, 129.4, 129.6, 129.9, 130.2, 130.8, 134.4, 136.0, 140.7, 147.5, 148.3, 148.4, 152.2, 152.9, 153.8, 154.4. Anal. Calcd for: $\text{C}_{87}\text{H}_{78}\text{N}_8\text{S}_2$: C, 80.40; H, 6.05; N, 8.62; S, 4.93. Found: C, 80.07; H, 6.52; N, 8.34; S, 5.13.

7. *(TPA-BTPy)Pt(pic)-Br*

A mixture of TPA-BTPy-Br (299 mg, 0.56 mmol), K_2PtCl_4 (155 mg, 0.37 mmol) in 2-ethoxyethanol (30 mL) and water (7 mL) was heated to 80 °C under stirring at nitrogen atmosphere for 12 h. After cooling to room temperature, the mixture was added to water (20 mL) and the resulting precipitate was collected and washed with water (20 mL \times 4) to provide dimer. This dimer was used for the next transformation without further purification. The mixture of dimer (254 mg, 0.167 mmol), picolinic acid (172 mg, 1.4 mmol), Na_2CO_3 (475 mg, 4.48 mmol) in 2-ethoxyethanol (30 mL) was stirred at 110 °C for 24 h under nitrogen atmosphere. The solvent was then removed under reduced pressure, and the residue was purified by flash chromatography using DCM-EtOH (*V/V*, 5:1) as the eluent to give a purplish red solid (116 mg, 41%). 1H NMR (400 MHz, $CDCl_3$), δ (ppm): 9.14 (d, $J = 5.1$ Hz, 1H), 8.88 (s, 1H), 8.67 (d, $J = 8.7$ Hz, 1H), 8.06 (t, $J = 7.4$ Hz, 1H), 7.98 (d, $J = 7.2$ Hz, 1H), 7.89 (d, $J = 8.3$ Hz, 2H), 7.71 (d, $J = 8.7$ Hz, 1H), 7.68 – 7.59 (m, 2H), 7.35 (t, $J = 7.6$ Hz, 4H), 7.23 (t, $J = 7.9$ Hz, 6H), 7.13 (t, $J = 7.2$ Hz, 2H). MALDI-MS (*m/z*): 851.418 for $[M^+]$.

8. (TPA-BTPy)Pt(pic)

(TPA-BTPy)Pt(pic) was synthesized referring to the synthetic procedure of (TPA-BTPy-Br)Pt(pic) and obtained as violet black powder in a yield of 33%. 1H NMR (400 MHz, DMSO) δ 9.23 (d, $J = 3.2$ Hz, 1H), 9.01 (d, $J = 4.6$ Hz, 1H), 8.94 (d, $J = 7.3$ Hz, 1H), 8.17 – 8.06 (m, 2H), 7.87 (d, $J = 7.7$ Hz, 2H), 7.77 (d, $J = 9.9$ Hz, 2H), 7.68 (s, 1H), 7.31 (d, $J = 7.0$ Hz, 4H), 7.22 (d, $J = 7.6$ Hz, 7H), 7.10 (t, $J = 6.5$ Hz, 2H), 6.97 (s, 1H). MALDI-MS (*m/z*): 772.204 for $[M^+]$.

9. (TPA-BTPy-Fl)Pt(pic)

(TPA-BTPy-Fl)Pt(pic) was synthesized referring to the synthetic procedure of (TPA-BTPy-Br)Pt(pic) and obtained as violet black powder in a yield of 28%. 1H

NMR (400 MHz, DMSO) δ 9.30 (s, 1H), 9.25 (s, 1H), 9.10 (s, 1H), 8.10 (s, 4H), 7.80 (d, J = 10.3 Hz, 6H), 7.63 (s, 2H), 7.59 (s, 1H), 7.48 (s, 1H), 7.38 (s, 2H), 7.31 (s, 4H), 7.21 (s, 4H), 7.10 (s, 2H), 1.55 (s, 6H). MALDI-MS (m/z): 964.318 for $[M]^+$.

10. *[Fl(TPA-BTPy)₂]Pt₂(pic)₂*

To a mixture of (TPA-BTPy)Pt(pic)-Br (104 mg, 0.122 mmol), 2-(9,9-dioctyl-7-(4,4,5,5-tetramethyl-1,3,2-dioxaborolan-2-yl)-9H-fluoren-2-yl)-4,4,5,5-tetramethyl-1,3,2-dioxaborolane (31 mg, 0.049 mmol) and Pd(PPh₃)₄ (6 mg) was added a degassed mixture of toluene (4 mL), tetrahydrofuran (2 mL) and 1 M cesium carbonate aqueous solution (1 mL). The mixture was refluxed for 18 h under the protection of nitrogen. The purified procedure was similar to that of TPA-BT-Br using DCM-EA (V/V , 4:1) as the eluent to give a purplish red solid (30 mg, yield 31%). ¹H NMR (400 MHz, CDCl₃), δ (ppm): 9.34 (s, 1H), 9.17 (d, J = 5.1 Hz, 2H), 9.07 (d, J = 8.2 Hz, 1H), 8.91 (d, J = 1.5 Hz, 2H), 8.70 (d, J = 8.7 Hz, 1H), 8.15 (d, J = 8.8 Hz, 1H), 8.09 – 8.02 (m, 4H), 7.98 (d, J = 7.3 Hz, 2H), 7.73 (d, J = 3.0 Hz, 2H), 7.69 – 7.59 (m, 8H), 7.37 (d, J = 6.9 Hz, 8H), 7.25 – 7.21 (m, 10H), 7.16 (t, J = 6.6 Hz, 8H), 2.27 – 2.07 (m, 4H), 1.39 – 1.06 (m, 24H), 0.81 (s, 6H). MALDI-MS (m/z): 1931.921 for $[M]^+$, 1955.879 for $[M + Na]^+$. Anal. Calcd for: C₉₉H₈₄N₁₀O₄Pt₂S₂: C, 61.54; H, 4.38; N, 7.25; S, 3.32 Found: C, 61.98; H, 3.91; N, 7.60; S, 3.63.

5. Acknowledgements

This work was supported by Financial support from the National Natural Science Foundation of China (51473140, 51273168, 21202139, 50973093), the Innovation Group in Hunan Natural Science Foundation (12JJ7002), the Scientific Research Fund of Hunan Provincial Education Department (10A119, 11CY023, 10B112), Natural Science Foundation of Hunan (12JJ4019, 11JJ3061), the Scientific Research

Fund of Xiangtan University (11QDZ18, 2011XZX08), and the Postgraduate Science Foundation for Innovation in Hunan Province (CX2012B249).

References

- 1) G. Qian, Z.Y. Wang. *Chem. Asian J.* 2010, **5**, 1006 - 1029.
- 2) H.F. Xiang, J.H. Cheng, X.F. Ma, X.G. Zhou, J.J. Chruma. *Chem. Soc. Rev.*, 2013, **42**, 6128 - 6185.
- 3) G. Lapadula, A. Bourdolle, F. Allouche, M.P. Conley, I. Rosal, L. Maron, W.W. Lukens, Y. Guyot, C. Andraud, S. Brasselet, C. Copéret, O. Maury, R. A. Andersen. *Chem. Mater.* 2014, **26**, 1062 - 1073.
- 4) D. Ding, K. Li, W. Qin, R.Y. Zhan, Y. Hu, J.Z. Liu, B.Z. Tang, B. Liu. *Adv. Healthcare Mater.* 2013, **2**, 500 - 507.
- 5) P.W. Jin, J. Chu, Y. Miao, J. Tan, S.L. Zhang, W.H. Zhu, *AIChE Journal*, 2013, **59**, 2743–2752
- 6) W.H. Wu, J.Z. Zhao, H.M. Guo, J.F. Sun, S.M. Ji, Z.L. Wang. *Chem. Eur. J.* 2012, **18**, 1961 - 1968.
- 7) G. Qian, Z. Zhong, M. Luo, D.B. Yu, Z.Q. Zhang, Z.Y. Wang, D.G. Ma, *Adv. Mater.* 2009, **21**, 111 - 116.
- 8) L. Guo, B. Yan. *Chem. Commun.* 2011, **14**, 1833 - 1837.
- 9) T.C. Lee, J.Y. Hung, Y. Chi, Y.M. Cheng, G.H. Lee, P.T. Chou, C.C. Chen, C.H. Chang, C.C. Wu. *Adv. Funct. Mater.* 2009, **19**, 2639 - 2647.
- 10) R. Tao, J. Qiao, G.L. Zhang, L. Duan, C. Chen, L.D. Wang, Y. Qiu. *J. Mater. Chem. C*, 2013, **1**, 6446 - 6454.
- 11) Y.F. Liu, W.H. Wu, J.Z. Zhao, X. Zhang, H.M. Guo. *Dalton Trans.*, 2011, **40**, 9085 - 9089.
- 12) X.G. Wu, Y. Liu, Y.F. Wang, L. Wang, H. Tan, M.X. Zhu, W.G. Zhu, Y. Cao. *Org.*

- Electron.* 2012, **13**, 932 - 937.
- 13) S.Q. Huo, J. Carroll, D. A. K. Vezzu, Design. *Asian J. Org. Chem.*, 2015, DOI: 10.1002/ajoc.201500246.
- 14) Z.Q. Guo, M.C.W. Chan. *Chem. Eur. J.* 2009, **15**, 12585 - 12588.
- 15) A.V. Soldatova, J. Kim, C. Rizzoli, M.E. Kenney, M.A.J. Rodgers, A.Rosa, G. Ricciardi. *Inorg. Chem.* 2011, **50**, 1135 - 1149.
- 16) K.R. Graham, Y.X. Yang, J.R. Sommer, A.H. Shelton, K.S. Schanze, J.G. Xue, J.R. Reynolds. *Chem. Mater.* 2011, **23**, 5305 - 5312.
- 17) T. Shigehiro, S. Yagi, T. Maeda, H. Nakazumi, H. Fujiwara, Y. Sakurai. *J. Phys. Chem. C*, 2013, **117**, 532 - 542.
- 18) S.C.F. Kui, F.F. Hung, S.L. Lai, M.Y. Yuen, C.C. Kwok, K.H. Low, S.S.Y. Chui, C.M. Che. *Chem. Eur. J.* 2012, **18**, 96 - 109.
- 19) H. Fukagawa, T. Shimizu, H. Hanashima, Y. Osada, M. Suzuki, H. Fujikake. *Adv. Mater.* 2012, **24**, 5099 - 5103.
- 20) C.J. Yang, C. Yi, M. Xu, J.H. Wang, Y.Z. Liu, X.C. Gao, J.W. Fu. *Appl. Phys. Lett.* 2006, **89**, 233506 - 233508.
- 21) H.F. Xiang, Z.X. Xu, V.A.L. Roy, B.P. Yan, S.C. Chan, C.M. Che, P.T. Lai. *Appl. Phys. Lett.* 2008, **92**, 163305 - 163307.
- 22) G. Qian, B. Dai, M. Luo, D.B. Yu, J. Zhan, Z.Q. Zhang, D.G. Ma, Z.Y. Wang, Band Gap Tunable. *Chem. Mater.* 2008, **20**, 6208 - 6216.
- 23) G. Qian, Z. Zhong, M. Luo, D.B. Yu, Z.Q. Zhang, D.G. Ma, Z.Y. Wang. *J. Phys. Chem. C* 2009, **113**, 1589 - 1595.
- 24) L. Yao, S.T. Zhang, R. Wang, W.J. Li, F.Z. Shen, B. Yang, Y.G. Ma. *Angew. Chem. Int. Ed.* 2014, **53**, 2119 - 2123.
- 25) S. Ellinger, K.R. Graham, P.J. Shi, R.T. Farley, T.T. Steckler, R. N. Brookins, P.

- Taranekar, J.G. Mei, L.A. Padilha, T.R. Ensley, H.H. Hu, S.Webster, D.J. Hagan, E.W.V. Stryland, K. S. Schanze, J. R. Reynolds. *Chem. Mater.* 2011, **23**, 3805 - 3817.
- 26) Y.X. Yang, R.T. Farley, T.T. Steckler, S.H. Eom, J.R. Reynolds, K.S. Schanze, J.G. Xue. *Appl. Phys. Lett.* 2009, **106**, 044509 - 044515.
- 27) T.T. Steckler, O. Fenwick, T. Lockwood, M.R. Andersson, F. Cacialli. *Macromol. Rapid Commun.* 2013, **34**, 990 - 996.
- 28) Z.Y. Hu, Y.F. Wang, D.Y. Shi, H. Tan, X.S. Li, L. Wang, W.G. Zhu, Y. Cao. *Dyes Pigments.* 2010, **86**, 166 - 173.
- 29) J.T. Yu, K.Q. He, Y.H. Li, H. Tan, M.X. Zhu, Y.F. Wang, Y. Liu, W.G. Zhu, H.B. Wu. *Dyes Pigments.* 2014, **107**, 146 - 152.
- 30) J. Luo, X.Z. Li, Q. Hou, J.B. Peng, W. Yang, Y.Cao. *Adv. Mater.* 2007, **19**, 1113 - 1117.
- 31) B.H. Zhang, C.J. Qin, J.Q. Ding, L. Chen, Z.Y. Xie, Y.X. Cheng, L.X. Wang. *Adv. Funct. Mater.* 2010, **20**, 2951 - 2957.
- 32) N.G. Connelly, W.E. Geiger. *Chem. Rev.* 1996, **96**, 877 - 910.
- 33) Y.M. Zhang, S.H. Wu, C.J. Yao, H.J. Nie, Y.W. Zhong. *Inorg. Chem.* 2012, **51**, 11387 - 11395.
- 34) C.J. Yao, J.N. Yao, Y.W. Zhong. *Inorg. Chem.* 2011, **50**, 6847 - 6849.
- 35) C. Lambert, G. Nöll. *J. Am. Chem. Soc.* 1999, **121**, 8434-8442.
- 36) H.J. Nie, C.J. Yao, M.J. Sun, Y.W. Zhong, J.N. Yao. *Organometallics* 2014, **33**, 6223 - 6231.
- 37) M. Renz, K. Theilacker, C. Lambert, M. Kaupp. *J. Am. Chem. Soc.* 2009, **131**, 16292 - 16302.
- 38) J.Y. Shao, W.W. Yang, J.N. Yao, Y.W. Zhong. *Inorg. Chem.* 2012, **51**, 4343 - 4351.

- 39) S.F. Li, G.Y. Zhong, W.H. Zhu, F.Y. Li, J.F. Pan, W. Huang, H. Tian, *J. Mater. Chem.*, 2005, **15**, 3221–3228.
- 40) S.Y. Chang, J. Kavitha, S.W. Li, C.S. Hsu, Y. Chi, Y.S. Yeh, P.T. Chou, G.H. Lee, A.J. Carty, Y.T. Tao, C.H. Chien. *Inorg. Chem.* 2006, **45**, 137 - 146.
- 41) Z.Q. Gao, B.X. Mi, H.L. Tam, K.W. Cheah, C.H. Chen, M.S. Wong, S.T. Lee, C.S. Lee. *Adv. Mater.* 2008, **20**, 774–778.

Figures and Tables

Figure 1. Molecular structures of (TPA-BTPy)Pt(pic), (TPA-BTPy-Fl)Pt(pic) and [Fl(TPA-BTPy)₂]Pt₂(pic)₂.

Scheme 1. Synthetic routes of (TPA-BTPy)Pt(pic), (TPA-BTPy-Fl)Pt(pic) and [Fl(TPA-BTPy)₂]Pt₂(pic)₂.

Figure 2. TGA curves of (TPA-BTPy)Pt(pic), (TPA-BTPy-Fl)Pt(pic) and [Fl(TPA-BTPy)₂]Pt₂(pic)₂.

Figure 3. Cyclic voltammograms of the (TPA-BTPy)Pt(pic), (TPA-BTPy-Fl)Pt(pic) and [Fl(TPA-BTPy)₂]Pt₂(pic)₂ films on platinum electrode in acetonitrile solution containing 0.1 mol L⁻¹ Bu₄NPF₆ at a scan rate of 100 mV s⁻¹.

Figure 4. UV-vis absorption spectra of (TPA-BTPy)Pt(pic), (TPA-BTPy-Fl)Pt(pic) and [Fl(TPA-BTPy)₂]Pt₂(pic)₂ in DCM (a) and in the neat films (b).

Figure 5. Normalized emission spectra of (TPA-BTPy)Pt(pic), (TPA-BTPy-Fl)Pt(pic) and [Fl(TPA-BTPy)₂]Pt₂(pic)₂ in DCM solution and neat films

Figure 6. UV-vis and NIR electronic absorption spectra of (TPA-BTPy)Pt(pic), (TPA-BTPy-Fl)Pt(pic) and [Fl(TPA-BTPy)₂]Pt₂(pic)₂ in dichloromethane after one electron oxidation by SbCl₅.

Figure 7. Isodensity plots of the calculated HOSO for three platinum complexes. All orbitals have been computed at an isovalue of 0.03.

Figure 8. EL spectra of the [Fl(TPA-BTPy)₂]Pt₂(pic)₂-doped PLEDs at dopant concentrations from 20 to 30 wt%.

Figure 9. The current density-voltage (*J-V*) and radiant emittance curves of the [Fl(TPA-BTPy)₂]Pt₂(pic)₂-doped PLEDs at different concentrations from 20 to 30

wt %.

Figure 10. The external quantum efficiency versus current density characteristics of the [Fl(TPA-BTPy)₂]Pt₂(pic)₂-doped PLEDs.

Table 1. Electrochemical and thermal parameters for (TPA-BTPy)Pt(pic), (TPA-BTPy-Fl)Pt(pic) and [Fl(TPA-BTPy)₂]Pt₂(pic)₂.

Table 2. Photophysical properties of (TPA-BTPy)Pt(pic), (TPA-BTPy-Fl)Pt(pic) and [Fl(TPA-BTPy)₂]Pt₂(pic)₂.

Table 3. The EL parameters of the [Fl(TPA-BTPy)₂]Pt₂(pic)₂-doped PLEDs.

Table 1

Compounds	$E_{\text{ox,onset}}/\text{V}^a$	$E_{\text{red,onset}}/\text{V}^a$	$E_{\text{HOMO}}/\text{eV}^b$	$E_{\text{LUMO}}/\text{eV}^b$	$E_{\text{cv}}^g/\text{eV}$	$T_{\text{d}}/^\circ\text{C}$
TPA-BTPy	0.98	-1.22	-5.63	-3.43	2.20	--
TPA- BTPy-FI	0.93	-1.17	-5.58	-3.48	2.10	--
FI(TPA-BTPy) ₂	0.77	-1.02	5.42	-3.67	1.79	--
(TPA-BTPy)Pt(pic)	1.07	-0.85	-5.72	-3.80	1.92	315
(TPA- BTPy-FI)Pt(pic)	1.06	-0.90	-5.71	-3.75	1.96	317
[FI(TPA-BTPy) ₂]Pt ₂ (pic) ₂	0.88	-0.93	-5.53	-3.72	1.81	296

^a Onset oxidation and reduction potentials measured by cyclic voltammetry in solid films;

^b $E_{\text{HOMO}} = -(E_{\text{ox}} - 0.45) - 5.1$ eV, $E_{\text{LUMO}} = -(E_{\text{red}} - 0.45) - 5.1$ eV, where 0.45 V is the potential for ferrocene vs. Ag/AgCl and 5.1 eV is the energy level of ferrocene to the vacuum energy level.

Table 2

Compound	$\lambda_{\text{abs, sol}}/\text{nm}$ ($\epsilon_{\text{max}}/10^4 \text{ L mol}^{-1} \text{ cm}^{-1}$) ^a	$\lambda_{\text{abs, film}}/\text{nm}$	$\lambda_{\text{onset, film}}/\text{nm}^b$	$E_{\text{g, film}}^{\text{opt}}/\text{eV}^c$	$\lambda_{\text{em, sol}}/\text{nm}$	$\lambda_{\text{em, film}}/\text{nm}$
(TPA-BTPy)Pt(pic)	311 (3.28); 429 (0.96); 492 (1.47)	503	581	2.13	643	601
(TPA-BTPy-FI)Pt(pic)	314 (4.91); 442 (1.77); 505 (2.29)	518	601	2.06	643	601
[FI(TPA-BTPy) ₂]Pt ₂ (pic) ₂	313 (7.84); 436(2.13); 507 (4.57)	523	605	2.05	643	603, 828

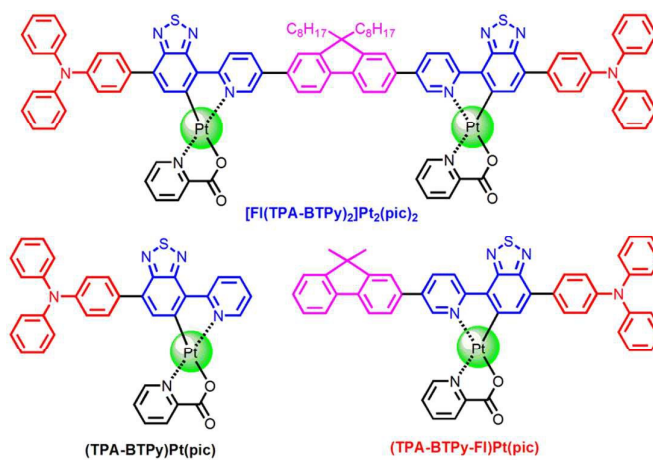
^a In dilute dichloromethane solution. ^b Absorption edges of the films. ^c Optical bandgaps were determined using the equation $E_{\text{g, film}}^{\text{opt}} = 1240/\lambda_{\text{onset, film}}$.

Table 3

Dopant (wt%)	$V_{\text{on}}(\text{V})^a$	$J(\text{mA cm}^{-2})^b$	$\lambda_{\text{EL}}(\text{nm})^c$	$R(\text{mW cm}^{-2})^d$	$\text{EQE}_{\text{max}}(\%)^e$
20	8.20	8.90	772	41	0.008
24	8.56	10.29	777	49	0.01
30	8.58	5.46	780	59	0.02

^a V_{on} : turn-on voltage at 1 cd cm^{-2} . ^b Current density at maximum EQE. ^c λ_{EL} : the maximum EL emission peak. ^d Radiant intensity. ^e EQE_{max} : the maximum external quantum efficiency.

Figure 1



Scheme 1

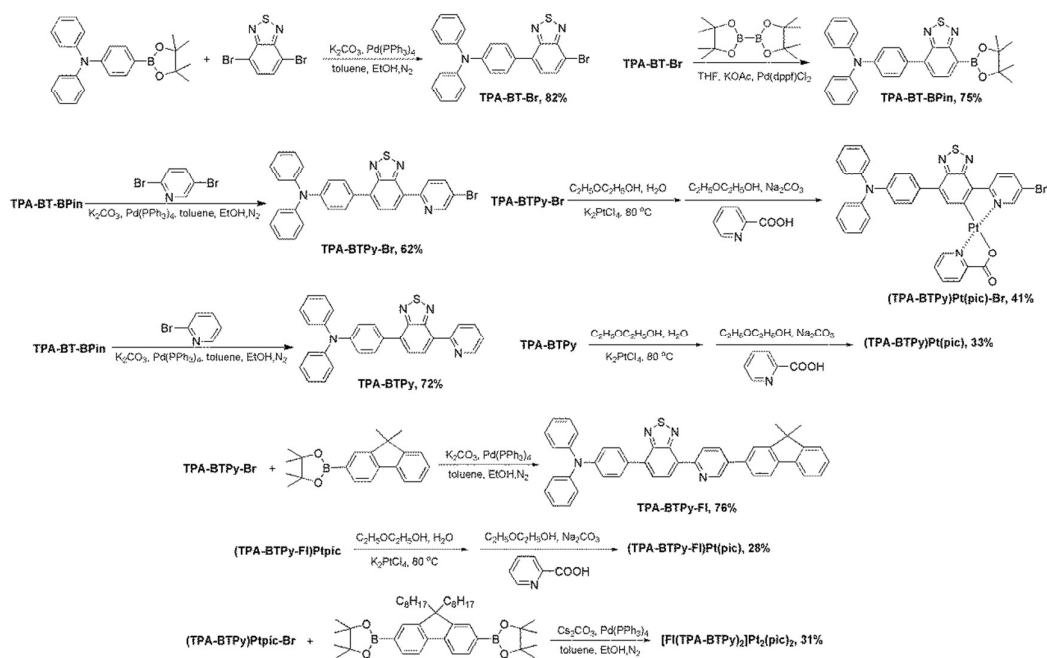


Figure 2

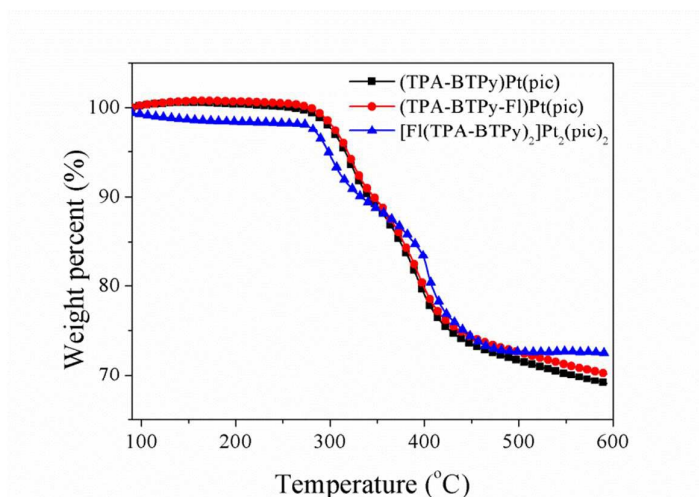


Figure 3

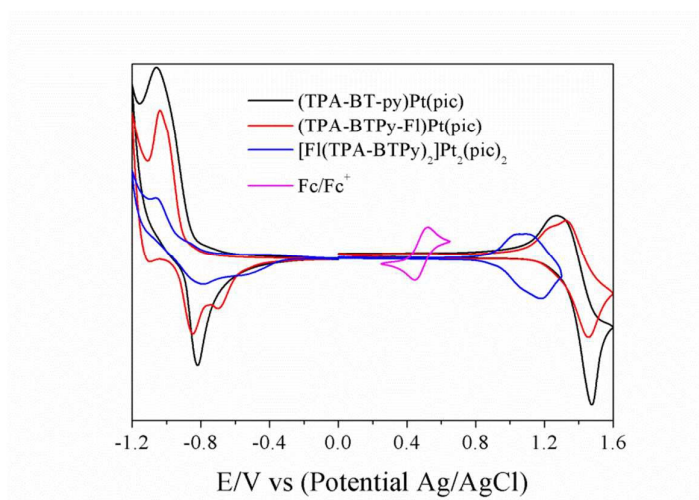


Figure 4

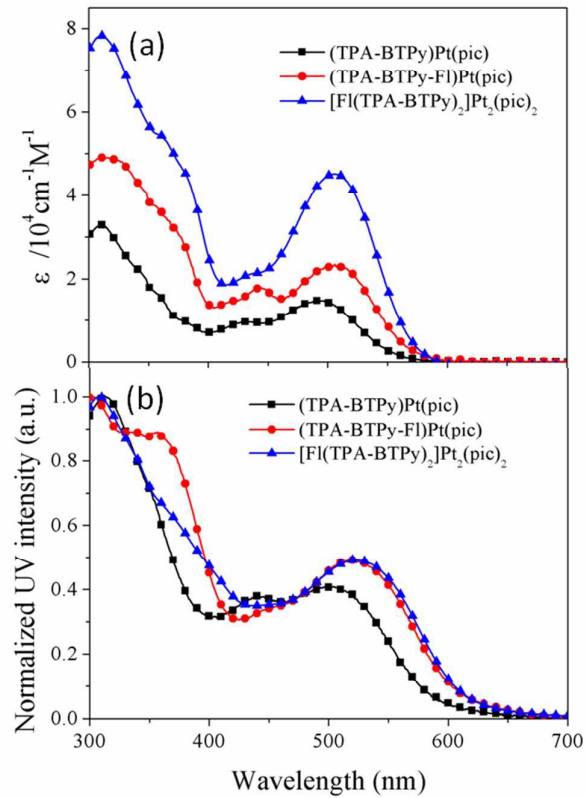


Figure 5

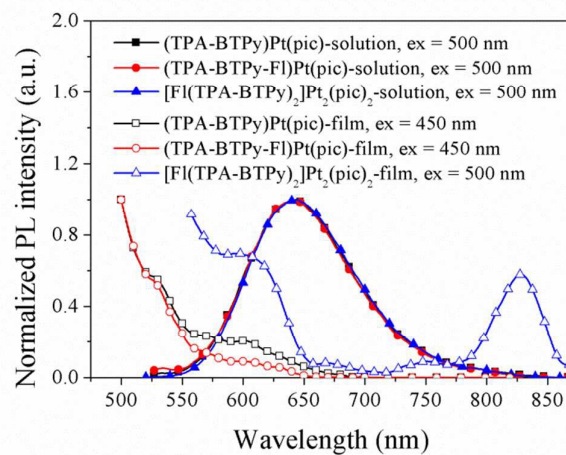


Figure 6

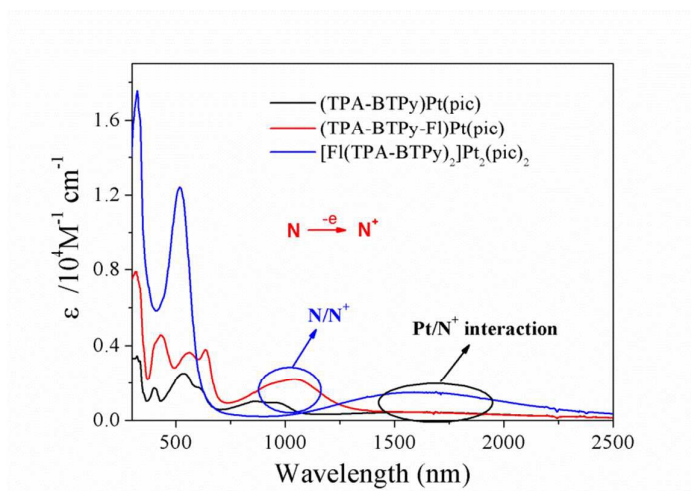


Figure 7

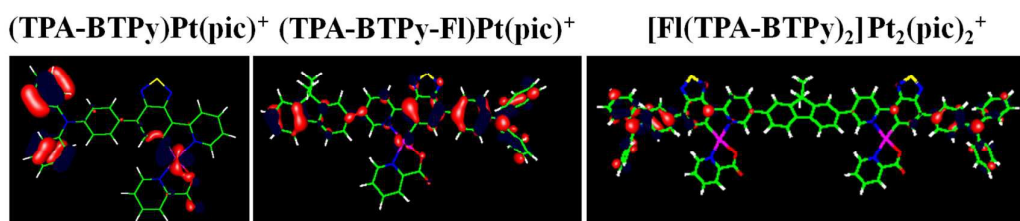


Figure 8

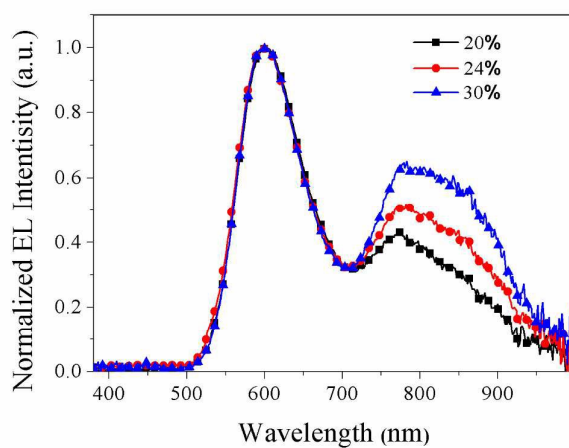


Figure 9

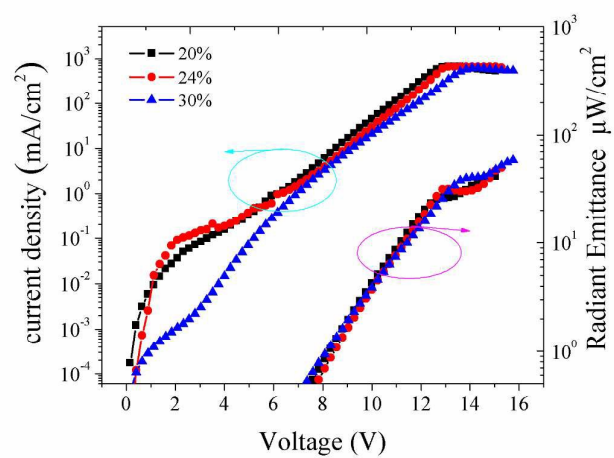
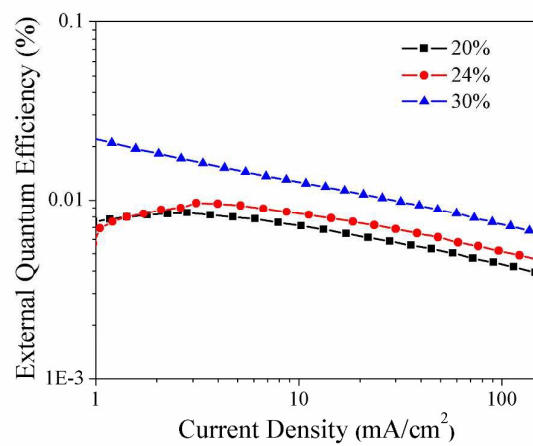


Figure 10



Graphical Abstract

Achieving near-infrared emission in platinum (II) complexes by using an extended donor-acceptor-type ligand

You-Ming Zhang, Fanyuan Meng, Jian-Hong Tang, Yafei Wang, Caifa You, Hua Tan,
Yu Liu, Yu-Wu Zhong, Shijian Su and Weiguo Zhu

Three D-A-type mononuclear and dinuclear platinum (II) complexes (TPA-BTPy)-Pt(pic), (TPA-BTPy-FI)Pt(pic) and [FI(TPA-BTPy)₂]Pt₂(pic)₂ were designed and obtained. By tuning the D-A framework, a dual emission peaked at 601 and 828 nm was observed only in the [FI(TPA-BTPy)₂]Pt₂(pic)₂-based film under photo-excitation. Under antimony pentachloride action, three platinum complexes presented one-electron oxidation and produced a different coupling intensity between ligand and platinum, which are consistent with their corresponding emission spectrum of Furthermore, using [FI(TPA-BTPy)₂]Pt₂(pic)₂ as dopant, its single-emissive-layer polymer light-emitting devices exhibited dual electroluminescence with a typical near-infrared peak of 780 nm and a red peak of 600 nm at a dopant concentration over 4 wt%. The maximum external quantum efficiency of 0.02% with a radiance of 59 $\mu\text{W}/\text{cm}^2$ was obtained in the device at 30 wt % dopant concentration.

